EPJ manuscript No.
(will be inserted by the editor)

Effect of volume fraction on chains of superparamagnetic colloids at equilibrium

A. Darras[1,2,3,a], E. Opsomer[1], N. Vandewalle[1], and G. Lumay[1]

[1] GRASP - Physics Department, University of Liège,
B-4000 Liège, Belgium
http://www.grasp-lab.org
[2] F.R.S.-FRNS,
B-1000 Bruxelles, Belgium
http://www.fnrs.be
[3] Experimental Physics, Saarland University,
D-66123 Saarbrücken, Germany
http://agwagner.physik.uni-saarland.de

Received: date / Revised version: date

Abstract. For a few decades, the influence of a magnetic field on the aggregation process of superparamagnetic colloids has been well known on short time scale. However, the accurate study of the equilibrium state is still challenging on some aspects. On the numerical aspect, current simulations have only access to a restricted set of experimental conditions due to the computational cost of long range interactions in many body systems. In the present paper, we numerically explore a new range of parameters thanks to sped up numerical simulations validated by a recent experimental and numerical study. We first show that our simulations reproduce results from previous study in well-established conditions. Then we show that unexpectedly long chains are observed for higher volume fractions and intermediate fields. We also present theoretical developments taking into account the interaction between the chains which are able to reproduce the data that we obtained with our simulations. We finally confirm this model thanks to experimental data.

PACS. 81.16.Dn Self-assembly – 47.57.J- Colloidal systems – 82.60.Lf Thermodynamics of solutions

1 Introduction

Self-assembly of superparamagnetic colloids has been a topic of intense research from a few decades [1–18]. Indeed, resulting structures can form microswarms or microswimmers useful for mixing in low Reynolds number or manipulate specific targets such as proteins, cells or bacteria, which leads to applications in waste capture, protein isolation, chromatography, bacteria processing, cell separation, etc. [4,7,10,18–32]. However, the previous studies often focus on the properties of such complex assemblies. The detailed formation process and the origin of those properties is still an open question. To our knowledge, the only system for which some model of growth has been published in the literature up to now is the colloidal chains formed under constant magnetic fields [12, 23,33–39]. The assembling mechanisms rely on the characteristic high magnetic response and quasi-zero residual magnetization of the building particles consisting of magnetic nanoparticles inserted in a matrix of non-magnetic material (polystyrene or silica) [17,18,23,35].

Given those properties, the particles interact magnetically as if they were perfect dipoles. Formally, let us consider the effective magnetic susceptibility χ of the particles and their volume $V = \frac{4}{3}\pi R^3$, given their radius R. Then, when an external magnetic field $\boldsymbol{B}$ is applied on the suspension, the particles acquire a magnetic dipole moment $\boldsymbol{\mu} = \chi V \boldsymbol{B}/\mu_0$. Actually, this equation is only valid for values far under the so-called magnetic saturation. With the paramagnetic materials we used, the magnetic field where this saturation is reached is of the order of 250 G [40,33,12]. Since we will consider only magnetic field of the order of 10 G, we will always stay in this linear regime for the considerations of this work. The interaction force, between two identical particles separated by a distance r, is therefore given by

$$\boldsymbol{F}_m = \frac{3\mu_0\mu^2}{4\pi r^4}((1-3\cos^2\theta)\boldsymbol{e_r} - \sin 2\theta \boldsymbol{e_\theta}), \qquad (1)$$

where θ is the angle between the line joining the centre of the particles and the magnetic field $\boldsymbol{B}$, $\boldsymbol{e}_r = \frac{\boldsymbol{r}}{r}$ and

Send offprint requests to: Alexis Darras
[a] *Corresponding author:* alexis.darras@uliege.be

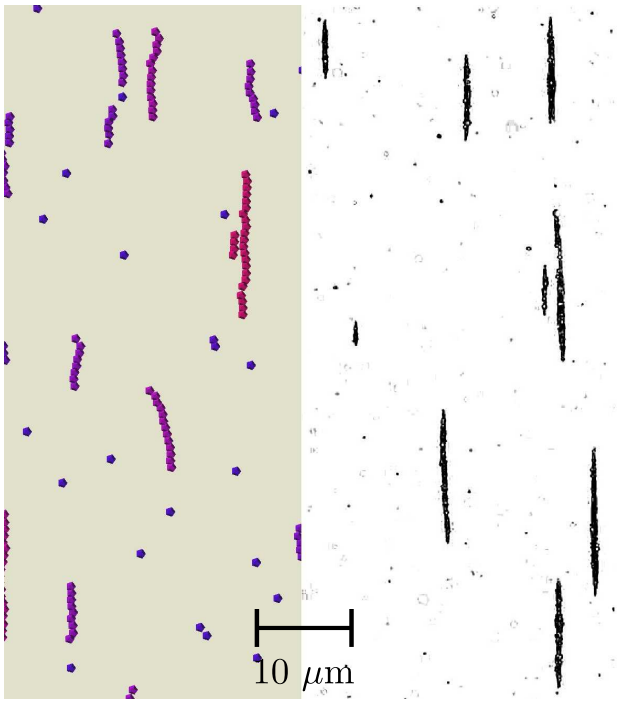

Fig. 1. Typical chains from numerical simulations (left) and experiments (right). Effective volume fraction of approximately $\phi_E = 0.015$.

$\boldsymbol{e}_\theta = \boldsymbol{e}_z \times \boldsymbol{e}_r$ if $\boldsymbol{e}_z$ is the unitary vector perpendicular to the plan containing $\boldsymbol{e}_r$ and $\boldsymbol{B}$. If $\boldsymbol{e}_r$ and $\boldsymbol{B}$ are parallel, $\theta = 0$ and the orientation of $\boldsymbol{e}_\theta$ is meaningless. Regarding the orientation of $\boldsymbol{F}_m$ and $\boldsymbol{r}$, if r points from particle 1 to particle 2, F is the force acting on particle 2. The subsequent magnetic interaction energy between those particles ($\boldsymbol{F}_m = -\boldsymbol{\nabla} U(r,\theta)$) is then

$$U(r,\theta) = \frac{\chi^2 4\pi R^6 B^2}{9\mu_0}\left(\frac{1-3\cos^2\theta}{r^3}\right), \qquad (2)$$

Two particles then repel each other if they are side-by-side, while they attract each other when they are aligned with the field $\boldsymbol{B}$. This interaction implies that two particles tend to aggregate aligned with the magnetic field $\boldsymbol{B}$. It has also been shown that the magnetic field produced by each particle influences the magnetic moments of their neighbours, through mutual induction [41]. However, this effect is significant only if the magnetic susceptibility is of the order of ferromagnetic materials. In this paper we used particles with magnetic susceptibility of $\chi \approx 0.1$, with SI units convention. In this situation, the mutual induction only modifies the magnetic moment of approximately one procent, while the value of Γ is modified by less than two procent. We can then neglect this effect. Note that, in this paper, the field will always be assumed to lie in the y direction, and the system is thin in the z direction (10 diameters of particles). As shown by several studies, both experimental and theoretical, superparamagnetic colloids self-organize into chains under those conditions, through diffusion-limited aggregation, as illustrated in fig.1 [34,42–45,27,46]. The characteristic dimensionless parameters governing this self-assembly are the volume fraction ϕ_0 and the ratio between the maximum of the magnetic energy and the thermal energy

$$\Gamma = \frac{\mu_0}{4\pi}\frac{\mu^2}{4R^3 k_B T} = \frac{\pi R^3 \chi^2 B^2}{\mu_0 9 k_B T}. \qquad (3)$$

Moreover, this aggregation is reversible, meaning that the chains break up if the magnetic field $\boldsymbol{B}$ is suppressed [12, 38]. Experimentally, chains of several particles are typically observed [34,44,42] and, after a transient behaviour, the growth is successfully described on short timescale (typically a few hundreds of seconds) by a Smoluchowsky equation, predicting a power law behaviour of the mean size of the chains $\langle s \rangle \propto t^z$ [34,42–45]. Current research usually focuses on more complex structures, looking like ribbons or bundles, that have been observed under those conditions [47,36] and new theoretical models are studied in order to take them into account and describe their properties [46,48,49]. On longer time scales, though, it has been shown that the system reaches a thermal equilibrium [23,35,47,36,39]. The saturation time varies between the instantness and tenths of years, depending on the volume fraction and the value of Γ [23]. For values of mean length at saturation $\langle s \rangle$ varying from unity to $\approx 10^2$, we previously observed experimental saturation time in the range of a few minutes to a few hours [36,39]. Up to now, the most convenient and efficient model for the mean length $\langle s \rangle$ of the agglomerates at thermal equilibrium has been established by Faraudo *et al.* [47]

$$\langle s \rangle = \sqrt{\phi_0 \ \exp\left(\Gamma - 1\right)}. \qquad (4)$$

Numerical simulations can be seen as useful tools to compare ideal experiments with actual experiments or theoretical expectations. Comparing with actual experiments can indicate if all the key physical ingredients are taken into account in the models. It can also be used to test some models in range of parameters which are not accessible experimentally. In the case of the analytical models for the mean chains length at saturation, [26,37] such simulations can (dis)confirm the mathematical approximations and the dependencies in the various parameters. However, classical techniques of numerical simulations (Langevin Dynamics, soft sphere discrete element methods, molecular dynamics, ...) would require several years of computing time to reach equilibrium state under some conditions: actual experiments last for hours and one second of simulation currently takes from 300 to 1100 hours of computering time. The most challenging situations are the ones leading to long chains, for which experiments and analytical models disagree [26,36,47]. Some researchers have developed alternative simulation techniques, where they consider the aggregation of the particles as irreversible and use a simplified magnetic interaction. This allows them to dynamically redefine the objects in the system and shorten the simulations by decreasing the numbers of objects to simulate [47]. However, those hypotheses are only valid when the magnetic interactions are really high and the system is diluted.

In the present work, we performed simulations with a modification of the viscosity of the surrounding fluid. We considered a fluid with a viscosity of $\eta = 2.5\ 10^{-5}\ Pa\,s$. As we showed in a previous work, above a certain threshold value, this doesn't fundamentally change the properties of the equilibrium of the system. [39] To validate our approach, we first begin to show that we indeed obtain the same results as with water ($\eta = 1\ 10^{-3}\ Pa\,s$) in well-known conditions. Afterwards, we numerically explore the equilibrium of high volume fractions systems, which could not be reached previously. We obtain unexpected high average lengths of the chains. We then demonstrate that interaction between chains can explain those results through a statistical approach. Eventually, we confirm the improvement of those theoretical considerations with actual experimental data.

2 Numerical simulations methods

In our study, simulations are realised using a Soft Sphere Discrete Element Method [50–52]. The code is the same as the one we developed for previous studies [39]. The algorithm progresses with a constant time step and solves Newton's equations of motion at each iteration. Regarding the involved forces, it takes into account the dipole-dipole interactions between the colloidal particles as well as the Brownian agitation in the system. In order to limit the computational cost, we introduced a cut-off distance for the magnetic dipole-dipole interaction, of about $12R$, by using a linked-cell method [53]. The random motion of a particle due to its interaction with surrounding fluid molecules in the heat bath can be described by using a Langevin equation [54]. To reproduce the effects of these interactions with the fluid, we then considered a drag force as $\boldsymbol{F}_d = -6\pi R\eta\boldsymbol{v}$, where $\boldsymbol{v}$ is the velocity of the particle. The Brownian force $\boldsymbol{F}_b$ is modeled as a Gaussian white noise process [55,56]. Regarding the collisions between particles, as well as collisions between a wall and a sphere, we model the normal contact force acting on two impacting objects as a linear spring-dashpot. We also take into account a tangential contact force, proportional to the relative slipping velocities of the particles and bounded by Coulomb's criterion. Furthermore, since sedimentation plays an important role in the dynamics of our system, gravity and buoyancy have to be included. Detailed equations for each force can be found in a previous publication [39].

It is worth noticing that changing the viscosity parameter η modifies both the drag force $\boldsymbol{F}_d$ and the Brownian force $\boldsymbol{F}_b$ in the simulations (indeed, $F_d \propto \eta$ and $F_b \propto \eta\sqrt{D} \propto \sqrt{\eta}$). Besides this, all the other parameters remain constant since they depend only on temperature and particle properties. In our simulations, we fixed the viscosity at $\eta = 25$ μPa.s, in order to speed up the simulations. [39] This value of the viscosity is fixing the Peclet number $Pe = \frac{R\chi^2}{36\mu_0}\sqrt{\frac{m}{3k_BT}}\frac{B^2}{\eta} \approx 0.11$ in a value largely below the critical Peclet number $Pe_C = 0.825$ we determined in an earlier work. [39] This should then guarantee that the equilibrium behaviour of the suspension is not modified by the change of viscosity, but represents a gain of a factor 40 on the simulation time. This gain would not be possible by simply increasing the time step of the simulations. Indeed, the time step intervals are fixed according to numerical stability of the collisions between particles. A safe value, not slowing down excessively the computation time, is given by $t_{step} = \frac{2\pi}{40}\sqrt{\frac{m}{k}}$, where m is the mass of the particles and k is the stiffness in the Hooke model for the particles collisions [50–52]. While increasing this time step by a factor 40 would lead to numerical instability of the collisions, decreasing the viscosity by this factor does not modify the evolution of the mean size of the system, as demonstrated in our previous work [39].

3 Numerical simulations results

We simulated systems within boxes with height $Z = 10\,\mu$m, width $X = 100\,\mu$m and length $Y = 400\,\mu$m. The magnetic field has a component only in the direction y of the length of the box $\boldsymbol{B} = B\boldsymbol{e}_y$, where $\boldsymbol{e}_y$ is the unitary horizontal vector parallel to the length Y of the box (the gravity being defined as $\boldsymbol{g} = -g\boldsymbol{e}_z$). While there is a periodic boundary condition on the vertical walls of the boxes (in order to limit the effect of the system size), the particles interact with the horizontal walls with the same contact forces as between two spheres. The fact that no further interaction is required to model real colloidal systems is supported by our previous experimental studies, where particles experience free diffusion near the wall [38].

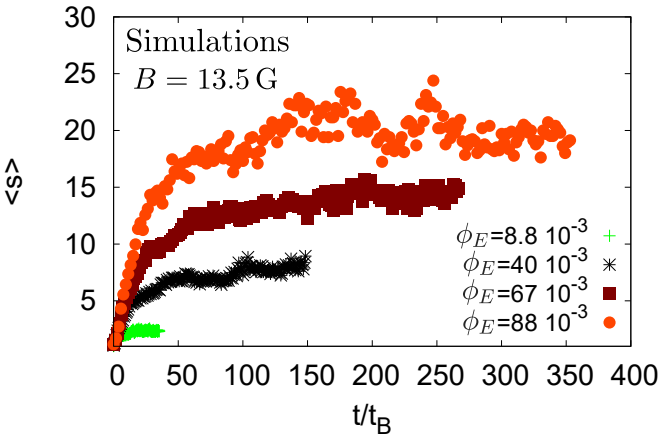

Fig. 2. Evolution of the mean size of the chains $\langle s\rangle(t)$ during simulations, for a magnetic field $B \approx 13.5\,$G ($\Gamma = 8$), and various effective volume fractions ϕ_E. The mean chains length is expressed in mean diameter of particles. The mean size of the chains is plotted as a function of the dimensionless parameter t/t_B.

Typical growth of the mean size of the chains along time $\langle s\rangle(t)$ is represented in fig. 2. The time has been adimensionalized by the characteristic time of aggregation of the particles $t_B = \frac{6\pi\eta R^3}{48\left[(1/3)^{1/2}-(1/3)^{3/2}\right]U_0\phi}$ [34,39]. As one

can see, the equilibrium state is reached after a characteristic time depending on the conditions of the simulations, as expected from previous works [23,26,36,39] . The rest of this section focus on the mean size of the chains at equilibrium, noted $\langle s \rangle$.

We first performed simulations in a range of volume fraction $\phi_0 = 1.15\ 10^{-3}$ and magnetic field $B \in [0; 21\ \mathrm{G}]$ (i.e. $\Gamma \in [0; 19]$) well characterized by previous studies. [26,23,47] In our system, we have to take into account the sedimentation. We then consider an effective sediment volume fraction of $\phi_E = \phi_0 \frac{h}{2R} = 8.8\ 10^{-3}$, computed by assuming the height available for the particles is their diameter $2R$, and where h is the height of the cell. When this value of volume fraction is injected in eq.(4), we obtain the expected saturation value for the mean length of the chains $\langle s \rangle$, as illustrated in fig. 3. This confirms the thermal equilibrium in our simulations is equivalent to the observed equilibrium in systems with higher viscosities.

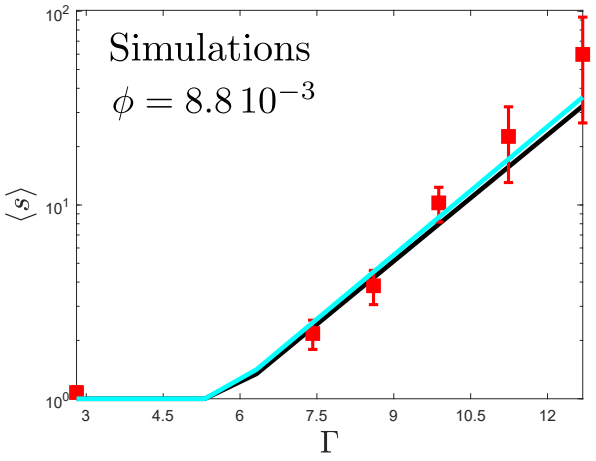

Fig. 3. Average lengths of the chains at saturation for various magnetic field with an effective sediment volume fraction $\phi_E = 8.8\ 10^{-3}$. Red points are data obtained from several numerical simulations. The black (lower) curve is the model of eq. (4) and the cyan (higher) curve is the model from eq.(9), with $K = 6/\pi$.

We also performed simulations for the same magnetic fields B and parameters Γ, but with a ten times higher volume fraction $\phi_0 = 11.5\ 10^{-3}$, or $\phi_E = 88\ 10^{-3}$. The results for those conditions are illustrated in fig. 4. As one can see, the model from eq.(4) systematically underestimates the mean length of the chains $\langle s \rangle$ in that particular situation. This highlights that a high volume fraction influences the mean length $\langle s \rangle$ in some way which has still to be understood.

In order to understand the role of the volume fraction, we then performed simulations with a fixed magnetic field $B = 13.5$ G and parameter $\Gamma = 8$, but various volume fraction ϕ_0 (and ϕ_E). The data from those simulations are represented in fig. 5. From these, we can see that the model from eq.(4) is accurate for sediment volume fractions up to $\phi_E = 2.6\ 10^{-2}$. However, for higher volume fractions, the

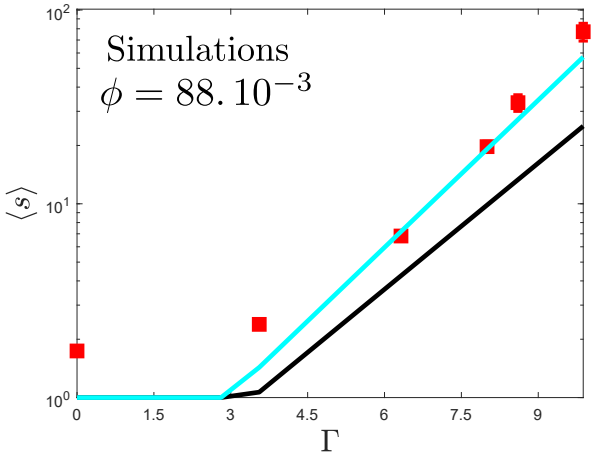

Fig. 4. Average lengths of the chains at saturation for various magnetic field with an effective sediment volume fraction $\phi_E = 88.\ 10^{-3}$. Red points are data obtained from several numerical simulations. The black (lower) curve is the model of eq. (4) and the cyan (higher) curve is the model from eq.(9), with $K = 6/\pi$.

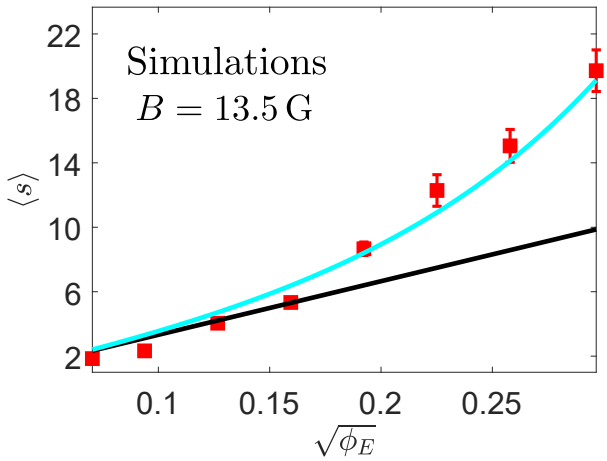

Fig. 5. Average lengths of the chains at saturation for various volume fraction with a magnetic field $B = 13.5$ G ($\Gamma = 8$). Red points are data obtained from several numerical simulations. The black line is the previous model (eq.(4)), while the blue (higher) curve is our new model (eq. (9)), with the value $K = 6/\pi$.

mean length at equilibrium $\langle s \rangle$ is higher than predicted by this law. Then, there must be some mechanism through which the volume fraction modifies this length. We discuss in the next section how the interaction between existing chains can be this mechanism.

We also measured the distribution of the chains' size obtained in our last set of simulations. As one can see in fig. 6, these distributions can be scaled thanks to predictions of the thermodynamic model (see section 4).

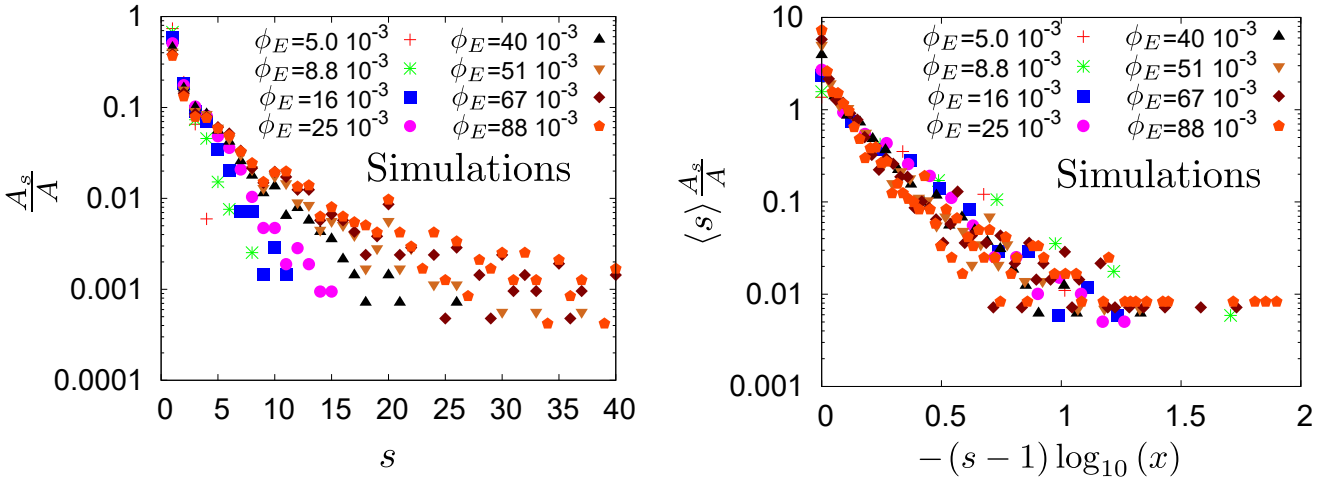

Fig. 6. Distribution of the chains' size s obtained with simulations, for various volume fraction and $\Gamma = 8$. Left: Normalized distribution of the number of chains A_s on the total number of chains A, for various effective volume fraction. Right: Scaling predicted by the models, with $\langle s \rangle$ being the actual mean size of the agglomerates at equilibrium and $x = (1 - 1/\langle s \rangle)$. With this scaling, predicted by both models, all the data collapse on the same curve. While we used a scaling closer to the model prediction, one can note from the left graph that the trend is the same as reported in previous studies [26].

4 Thermodynamic model

The previous model (eq. (4)) is based on thermodynamics development where the thermal equilibrium determines the homogeneity of the chemical potential of every particle. This model can then be easily modified if one finds a dependency of the chemical potential as a function of the volume fraction. For this purpose, we consider the expression of the chemical potential μ_s for a chain of s colloidal particles

$$\mu_s = \mu_s^0 + \frac{1}{s}\left[k_B T \ln \frac{\phi_s}{s}\right] \tag{5}$$

where μ_s^0 is the mean free-energy per particle and the second term comes from the entropy, with ϕ_s being the volume fraction of the chains of lengths s (see Eqs. (19.1) and (19.6) in Ref. [57], and development in Ref. [47]). The model leading to eq.(4) has been established by considering that the energy of a chain of s colloids with a magnetic bond energy $-\epsilon$ is $-(s-1)\epsilon$. This gives $\mu_s^0 = \mu^0 - (s-1)\epsilon/s$. [47,57]. In 3D, the bond can be assessed as $\beta\epsilon \approx \Gamma - 1$, where $\beta = 1/(k_B T)$, from a mean-field hypothesis. We discuss in Appendix 7 the difference between 2D and 3D models and show that the 3D model has to be used in our case.

In order to have a further effect of the volume fraction, we suggest considering the interaction between the chains of colloids. We will here introduce a reasoning to apply another mean-field theory to this interaction. Let us consider the case of long chains created in a high volume fraction suspension. We can idealize the system as a succession of parallel chains separated by a mean distance d. If we assume that the chains are long compared to their distance d, we can assimilate these chains to magnetic needles whose interacting energy U_{CC} behaves like

$$U_{CC} = \frac{\mu_0}{4\pi}\frac{\mu^2}{4R^2}\frac{2}{d}, \tag{6}$$

see eq.(16) in Ref. [58]. By considering the sedimentation, the available volume for each particle goes like $\tilde{V} \approx d4R^2$, while their own volume is $V_p = 4\pi R^3/3$. The total sediment volume fraction is then $\phi_E = V_p/\tilde{V} = (\pi R)/(3d)$. This leads the average distance d between the chains to be $d = (\pi R)/(3\phi_E)$. Then, each chain has a repulsive interaction with its two neighbours, creating an interaction energy per chain

$$U_{CC} = \frac{\mu_0}{4\pi}\frac{\mu^2}{4R^2}\frac{6\phi_E}{\pi R} = \frac{6}{\pi}\Gamma k_B T \phi_E \equiv K\, k_B T\, \Gamma\, \phi_E, \tag{7}$$

where $K = \frac{2R}{d\phi_E}$ is a geometric constant that our idealization approximates as $K \approx 6/\pi$. The chemical potential of the particles can then eventually be expressed as

$$\mu_s = \mu^0 + \frac{1}{s}\left[k_B T \ln\left(\frac{\phi_s}{s}\right) - (s-1)\epsilon + K\, k_B T\, \Gamma\, \phi_E\right]. \tag{8}$$

Then, a reasoning perfectly analogous to the one of Faraudo *et al.* [26], based on the equilibrium of the chemical potential $\mu_1 = \mu_s$ and the constraint $\phi_E = \sum_s \phi_s$, leads to

$$\langle s \rangle = \sqrt{\phi_E \exp\left(\Gamma - 1 + K\Gamma\phi_E\right)}. \tag{9}$$

This model has been represented in fig. 5. The value of $K = 6/\pi$ gives the blue curve. As can be seen in the graph, this curve has the right trend and is in good agreement with the numerical data.

Moreover, the curve corresponding to eq. (9), with $K = 6/\pi$, has been represented on the figs. 3 and 4. Indeed, eq. (9) also shows a different dependency on Γ than eq. (4). For the case of low volume fraction (fig. 3), both models give pretty similar results, in good agreement with the numerical data. In the case of high volume fraction (fig. 4), both models fail to explain the low Γ data, but eq. (9) is in good agreement with the numerical data for higher Γ. Actually, such a deviation in

the beginning of the data is due to an increased probability of random collisions between particles which create temporary aggregates. Those agglomerates are formed by particles whose contact time is directly controlled by the collision of the particles and are not sticking together due to magnetic interactions. Of course, this can only occur in low Γ configuration, and they are not taken into account in the equilibrium ensemble of the models, because it is not the competition between their magnetic and thermal energy which creates the agglomerate, but rather geometrical constraints (i.e. the space available for each particle during their free diffusion). For instance, some of these agglomerates can be oriented perpendicularly to the magnetic field, which is not considered in the equilibrium model, given their repulsive magnetic interaction. Actually, the model computing $\beta\epsilon \approx \Gamma - 1$ considers only chains constituted of particles whose angles between their magnetic moment (in the direction of the external field) and the direction pointing to the centre of their closest neighbours is comprised between $-\theta_0$ and θ_0, where $\theta_0 = \arcsin\sqrt{2/3}$, so that the radial component of the magnetic interaction is attractive. Moreover, the analytical expression of both models have been obtained with approximations assuming that Γ and the predicted value of the average chains length are large in front of 1. (see eqs. (6) and (7) in Ref. [26]). Furthermore, the configuration of parallel long chains leading to eq. (9), which can happen only with an important magnetic field, or Γ, is not suitable to describe a system composed of small agglomerates. The expression of U_{CC} in eq. (7) has explicitly been obtained by assuming that the length of the chains is longer than their distance (see Ref. [58]) which means $d > \langle s\rangle R \Leftrightarrow \phi_E\langle s\rangle > \pi/3$. Since the effective volume fraction we used is of the order of $\phi \approx 0.1$, this is another reason why our model becomes accurate for values of $\langle s\rangle \gtrsim 10$. The agreement with only the high Γ points is then not surprising. For lower volume fraction, however, the term $K\Gamma k_B T\phi_E$ is often negligible to $\Gamma - 1$ and does not modify too much the predicted value (as illustrated in fig. 3).

The distribution of the chains size obtained in our simulations is represented in the fig. 6. To compare with the models, one can note that both models imply that the number A_s of chain with length s is proportional to $A_s \propto \phi_s/s \propto x^s$, where $x = \phi_1 \exp(\Gamma - 1 + K\Gamma\phi_E)$ in our case and $x = \phi_1 \exp(\Gamma - 1)$ in the previous model. From this, it comes that the normalized distribution of the chains A_s/A, with $A = \sum_{s=1}^{+\infty} A_s$ behaves like $A_s/A = (1-x)x^{s-1}$. In the limit $\langle s\rangle >> 1 \Rightarrow x \approx (1 - 1/\langle s\rangle)$, leading to eqs. (4) and (9), we can then write $\log_{10}(\langle s\rangle A_s/A) = (s-1)\log_{10} x$. The mean size of particles at equilibrium is then the only relevant parameter in the system, since it determines the distribution of the particles. While the finite size of the systems we simulated prevent the data to exactly follow this relation, it can still be used as an efficient scaling law to collapse all the data on a same master curve, as illustrated in fig. 6.

In order to confirm those theoretical considerations, we also performed actual experiments described in the next section.

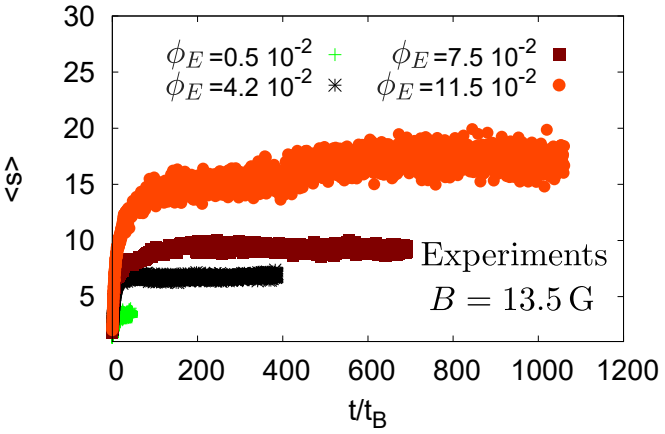

Fig. 7. Evolution of the mean size of the chains $\langle s\rangle(t)$ during experiments, for a magnetic field $B \approx 13.5$ G, and various effective volume fraction ϕ_E. The mean chains length is expressed in mean diameter of particles. The mean size of the chains is plotted as a function of the dimensionless parameter t/t_B.

5 Experimental setup

A part of a typical experimental picture is presented in fig. 1. The experiments were performed with superparamagnetic microspheres dispersed in water (Estapor® M1-070/60), with a volumic fraction varying from $\phi_0 = 1.\,10^{-4}$ to $\phi_0 = 23.\,10^{-4}$ ($\phi_E = 5.\,10^{-3}$ to $\phi_E = 115.\,10^{-3}$). The suspension was placed inside a cylindrical chamber of diameter $D = 5$ mm and thickness approximately $h = 50$ μm. The chamber was formed by two parallel glass plates. The first glass plate was covered with an approximately 50 μm layer of epoxy with the exemption of a circular region. A suspension droplet of 1 μl was placed inside this region. Afterwards, the second glass plate was placed on the first one. A small quantity of low-viscosity silicon oil was placed on the epoxy to assess the watertightness of the chamber. A constant and homogeneous magnetic field $B \approx 13.5$ G was generated by a constant current in surrounding coils at the beginning of each experiment. The magnetic field produced by those coils was characterized with a Hall probe and was homogeneous within the precision range of the probe of 2% around the cell. The current in the coils had a constant intensity controlled by a programmable DC power supply GenH-750W from TDK Lambda, with a precision of 0.01 A. The suspension was observed from the bottom with a 40x magnification. The microscope used was an inverted microscope Olympus IX73, connected to a 4070M-CL Thorlabs Camera with 2048 by 2048 pixels of 16 Bits depth. The images were recorded with a frame rate of 1fps during ten minutes, then a frame rate of 0.1 fps is applied. Each experiment lasted between five and eight hours. Experiments

were performed at least three times for each condition in order to assess reproducibility of the results.

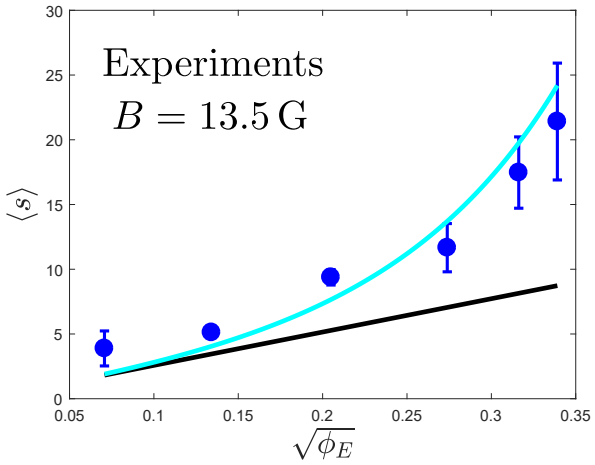

Fig. 8. Equilibrium mean size of the particles as a function of effective volume fraction ϕ_E. The circles are experimental measurements while the curves are the models. The black line is the prediction from eq.(4), while the cyan curve is a prediction of our model (eq.(9)), with $K = 6/\pi$. Both models used $\Gamma = 7.25$.

6 Experimental validation

Experimental growth of the mean size of the chains along time $\langle s \rangle(t)$ is represented in fig. 7. As for the simulations, the time has been adimensionalized by the characteristic time of aggregation of the particles t_B. As one can see, the equilibrium state is again reached after a characteristic time depending on the conditions of the experiments. The rest of this section focuses on the mean size of the chains at equilibrium, noted $\langle s \rangle$.

The measured equilibrium mean size of the particles as a function of effective volume fraction is shown in fig. 8. The range of plausible $\Gamma = \frac{\pi R^3 \chi^2 B^2}{\mu_0 9 k_B T}$, we obtained from the mean properties of the particles and their uncertainty is $\Gamma \in [6.6; 7.9]$, giving $\Gamma = 7.25 \pm 0.65$.

One can see that eq. (9), considering $K = 6/\pi$ and $\Gamma = 7.25$, gives a trend consistent with the experimental data. The agreement of the data with eq. (9) is even better than the agreement with the predictions of eq. (4).

The experimental distribution of chains size is illustrated in fig. 9. These distributions contain more noise (mainly due to image analysis) and are as clearly separated than the ones obtained with the simulations. However, the previous scaling $\log_{10}(\langle s \rangle A_s/A) = (s-1)\log_{10} x$ still collapse all the data on the same curve.

7 Conclusions

Compared with the previous numerical studies of Faraudo *et al.* [26,23,47], our work report systematic experiments to assess the theoretical models. We also characterized suspensions with a higher range of volume fraction than these works, and modified systematically this parameter. Furthermore, our simulations and experiments demonstrated that the current model (eq. (4)) regarding the equilibrium length of superparamagnetic colloids under magnetic field does not reproduce the adequate volume fraction dependency. Indeed, we identified the ignored interactions between the chains as a cause of divergence between this model and both numerical and experimental data. Moreover, we showed that idealizing assumptions could lead to a consistent model. We showed this modification is not only important when only the volume fraction is varying, but also when considering a high volume fraction system and varying the characteristic interaction energy of the particles (i.e. by varying Γ by any means). Accordingly, this work opens new perspectives to model and understand such high volume fraction systems.

Acknowledgements

A.D. is financially supported by FNRS as research fellow. This work was financially supported by the FNRS (Grant PDR T.0043.14) and by the University of Liège (Starting Grant C-13/88). E.O. acknowledges financial support by the European Space Agency and Belspo (Prodex) via the VipGran Project. Authors thank Charlotte Marique for spell-checking the manuscript.

Author contributions statement

GL and AD conceived the experiments, AD conducted the experiments, EO and AD conceived the simulation code, EO wrote the simulation code, AD managed the simulations, EO and AD wrote the manuscript. AD and NV built the theoretical model. AD, EO, GL and NV analyzed the results and reviewed the manuscript.

Additional information

The datasets generated during and/or analysed during the current study are available from the corresponding author on reasonable request.

Appendix A. Dimensionality of the models

We used a 3D model for the aggregation instead of a 2D model, even if the particles sediment in our simulations and experiments. Indeed, as we demonstrated in a previous work [36], there are two ways Faraudo's model should be modified to take a change of dimension into account.

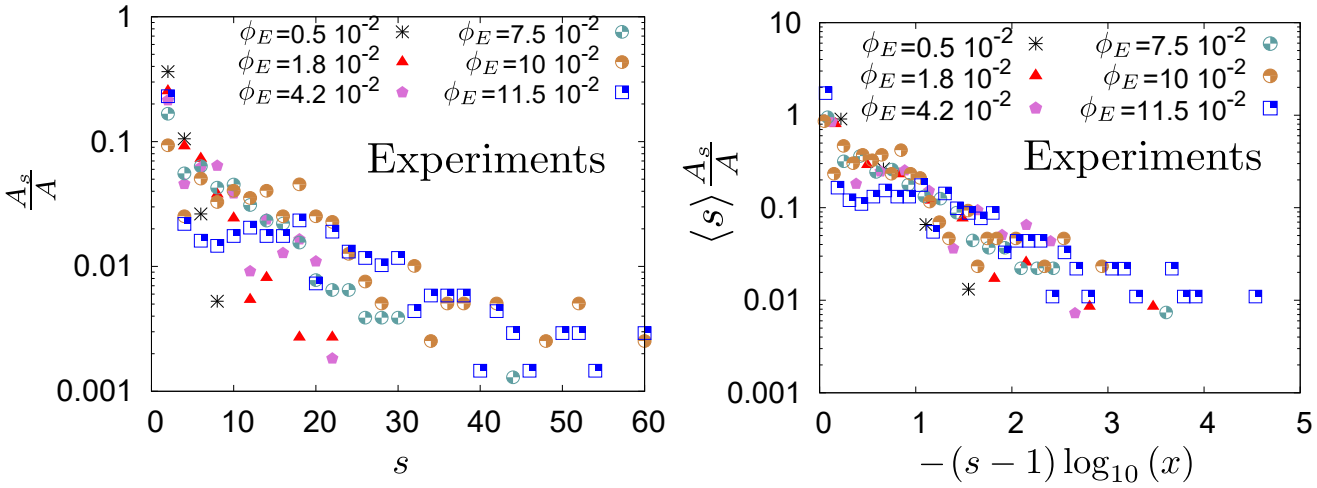

Fig. 9. Distribution of the chains of size s obtained in experiments, for various volume fraction and a constant magnetic field $B \approx 13.5$ G. Left: Normalized distribution of the number of chains A_s on the total number of chains A, for various effective volume fraction. Right: Scaling predicted by the models, with $\langle s \rangle$ being the actual mean size of the agglomerates at equilibrium and $x = (1 - 1/\langle s \rangle)$. With this scaling, predicted by both models, all the data collapse on the same curve.

The first one is that the surface fraction $\phi_S^{2D} \equiv \frac{N\pi R^2}{A}$, where N is the number of particles, R their radius and $A = XY$ the area of the bottom plate, should be used instead of the volume fraction. The second way the model should be modified is through the effective mean bond energy ϵ. This parameter is related to Γ through a thermodynamic mean value of the magnetic interaction energy, and makes use of a Jacobian depending on the dimensionality. Introducing the right 2D configuration space in the computations of Faraudo *et al.*[26] leads to $\beta\epsilon^{2D} = \Gamma - 1/2$ [36]. We then have a final model $\langle s \rangle = \sqrt{\phi_S^{2D} \exp(\Gamma - 1/2)}$.

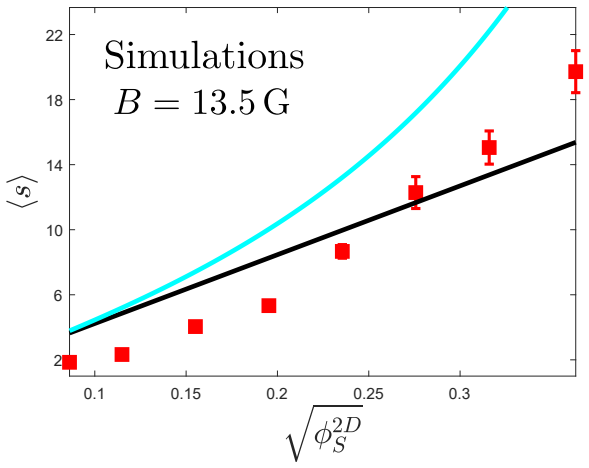

Fig. 10. Average lengths of the chains at saturation for various surface fraction with a magnetic field $B = 13.5$ G ($\Gamma = 8$). Red points are data obtained from several numerical simulations. The black line is the 2D version of Faraudo's model , while the blue (higher) curve is the 2D version of our new model, with the approximate value $K = 4/\pi$.

However, as illustrated in fig.10 when we compared this model with our data, it does not catch their trend at all... While the 3D version of Faraudo's model actually predicts efficiently the saturation values, once we used the effective volume fraction ϕ_E in the vicinity of the sedimented particles (which differs from the 2D surface fraction by a factor 2/3 $\phi_E = \frac{N4\pi R^3}{3XY2R} = \frac{2}{3}\phi_S^{2D}$), as it does for the case of data in fig. 3 (which has been obtained in conditions similar to those for which the model has been developed).

Similarly, our proposition and the computation of d and K would depend on the dimensionality. In 2D, the available surface for each particle would go like $\tilde{A} \approx 2Rd$ while their own surface is πR^2. The mean distance d would then be obtained through $\phi_S^{2D} = \frac{\pi R}{2d} \Rightarrow d = \frac{\pi R}{2\phi_S^{2D}}$ leading to $K = \frac{4}{\pi}$ to write $U_{CC} = K\, k_B T \Gamma \phi_S^{2D}$.

As can be seen from fig.10, none of the 2D curves match any part of the data's trend. One should not be surprised that the 2D models do not efficiently predict what happens in our simulations, which are as close as possible to our experiments. Indeed, the particles are not strictly restricted to a 2D plane : the thermal energy of the system is approximately equal to $mg2R$, with m the mass of the particles, allowing single particles to elevate their centre of mass over another particle. This means that collisions between particles are actually 3D. Since the volume fraction influences the mean size of the chains through their probability of collisions, this explains why one has to take into account the volume fraction of the particles in the sedimented layer and not their surface fraction. Moreover, this thermal agitation makes that no solid constraint restricts the elevation between two neighbouring particles. Then, the same configuration space is available for the particles as in 3D (contact between two particles is still defined through a surface, not through a curve). Since this configuration space determines the properties of the systems at equilibrium, it is then not surprising that it is the same as predicted by a 3D model. While the kinetics lead-

ing to this equilibrium might differ (since approximately one half of the path leading to aggregation are missing compared to pure 3D cases), there are no reasons why the equilibrium state should be considered to be 2D.

References

1. J. Yu, B. Wang, X. Du, Q. Wang, L. Zhang, Nature communications **9**, 3260 (2018)
2. K. Müller, N. Osterman, D. Babič, C.N. Likos, J. Dobnikar, A. Nikoubashman, Langmuir **30**, 5088 (2014)
3. M. Llera, J. Codnia, G.A. Jorge, J. Magn. Magn. Matter **384**, 93 (2015)
4. R.M. Erb, H.S. Son, B. Samanta, V.M. Rotello, B.B. Yellen, Nature **457**, 999 (2009)
5. H. Löwen, Journal of Physics: Condensed Matter **20**, 404201 (2008)
6. V. Froltsov, R. Blaak, C. Likos, H. Löwen, Physical Review E **68**, 061406 (2003)
7. F. Martinez-Pedrero, P. Tierno, Phys. Rev. Applied **3**, 051003 (2015)
8. F. Martinez-Pedrero, A. Ortiz-Ambriz, I. Pagonabarraga, P. Tierno, Phys. Rev. Lett. **115**, 138301 (2015)
9. H. Carstensen, V. Kapaklis, M. Wolff, Phys. Rev. E **92**, 012303 (2015)
10. P. Liu, J.W. De Folter, A.V. Petukhov, A.P. Philipse, Soft Matter **11**, 6201 (2015)
11. D.L. Blair, A. Kudrolli, Physical Review E **67**, 021302 (2003)
12. P. Domínguez-García, J. Pastor, M. Rubio, Eur. Phys. J. E **34**, 1 (2011)
13. P. Domínguez-García, S. Melle, J. Pastor, M. Rubio, Phys. Rev. E **76**, 051403 (2007)
14. S. Merminod, T. Jamin, E. Falcon, M. Berhanu, Physical Review E **92**, 062205 (2015)
15. K.V. Edmond, H. Park, M.T. Elsesser, G.L. Hunter, D.J. Pine, E.R. Weeks, Chaos-Woodbury **21**, 041103 (2011)
16. R. Dreyfus, J. Baudry, M.L. Roper, M. Fermigier, H.A. Stone, J. Bibette, Nature **437**, 862 (2005)
17. J.W. Tavacoli, P. Bauër, M. Fermigier, D. Bartolo, J. Heuvingh, O. du Roure, Soft Matter **9**, 9103 (2013)
18. U. Jeong, X. Teng, Y. Wang, H. Yang, Y. Xia, Adv. Mater. **19**, 33 (2007)
19. J.L. Corchero, A. Villaverde, Trends Biotechnol. **27**, 468 (2009)
20. B. Kozissnik, A.C. Bohorquez, J. Dobson, C. Rinaldi, International Journal of Hyperthermia **29**, 706 (2013)
21. Q. Pankhurst, N. Thanh, S. Jones, J. Dobson, Journal of Physics D: Applied Physics **42**, 224001 (2009)
22. M. Colombo, S. Carregal-Romero, M.F. Casula, L. Gutiérrez, M.P. Morales, I.B. Böhm, J.T. Heverhagen, D. Prosperi, W.J. Parak, Chemical Society Reviews **41**, 4306 (2012)
23. J. Faraudo, J.S. Andreu, J. Camacho, Soft Matter **9**, 6654 (2013)
24. C.T. Yavuz, J. Mayo, W.Y. William, A. Prakash, J.C. Falkner, S. Yean, L. Cong, H.J. Shipley, A. Kan, M. Tomson et al., Science **314**, 964 (2006)
25. K.M. Krishnan, IEEE Trans. Magn. **46**, 2523 (2010)
26. J.S. Andreu, J. Camacho, J. Faraudo, Soft Matter **7**, 2336 (2011)
27. G.P. Gajula, M.T. Neves-Petersen, S.B. Petersen, Appl. Phys. Lett. **97**, 103103 (2010)
28. K.S. Khalil, A. Sagastegui, Y. Li, M.A. Tahir, J.E. Socolar, B.J. Wiley, B.B. Yellen, Nat. Commun. **3**, 794 (2012)
29. Y. Gurevich, Y. Mankov, R. Khlebopros, Dokl. Phys. **11**, 478 (2013)
30. F. Martinez-Pedrero, P. Tierno, Phys. Rev. Applied **3**, 051003 (2015)
31. H. Carstensen, V. Kapaklis, M. Wolff, Phys. Rev. E **92**, 012303 (2015)
32. C.T. Yavuz, A. Prakash, J. Mayo, V.L. Colvin, Chem. Eng. Sci. **64**, 2510 (2009)
33. P. Domínguez-García, S. Melle, J. Pastor, M. Rubio, Physical Review E **76**, 051403 (2007)
34. J.H. Promislow, A.P. Gast, M. Fermigier, J. Chem. Phys. **102**, 5492 (1995)
35. J. Faraudo, J. Camacho, Colloid Polym. Sci. **288**, 207 (2010)
36. A. Darras, J. Fiscina, M. Pakpour, N. Vandewalle, G. Lumay, The European Physical Journal E **39**, 1 (2016)
37. N. Rojas, A. Darras, G. Lumay, Physical Review E **96**, 012608 (2017)
38. A. Darras, J. Fiscina, N. Vandewalle, G. Lumay, American Journal of Physics **85**, 265 (2017)
39. A. Darras, E. Opsomer, N. Vandewalle, G. Lumay, Scientific reports **7**, 7778 (2017)
40. M. Fermigier, A.P. Gast, Journal of colloid and interface science **154**, 522 (1992)
41. H. Zhang, M. Widom, Physical Review E **51**, 2099 (1995)
42. S. Fraden, A.J. Hurd, R.B. Meyer, Phys. Rev. Lett. **63**, 2373 (1989)
43. M. Kolb, Phys. Rev. Lett. **53**, 1653 (1984)
44. F. Martínez-Pedrero, M. Tirado-Miranda, A. Schmitt, J. Callejas-Fernández, Phys. Rev. E **76**, 011405 (2007)
45. S. Miyazima, P. Meakin, F. Family, Phys. Rev. A **36**, 1421 (1987)
46. H. Ezzaier, J. Alves Marins, I. Razvin, M. Abbas, A. Ben Haj Amara, A. Zubarev, P. Kuzhir, The Journal of Chemical Physics **146**, 114902 (2017)
47. J. Faraudo, J.S. Andreu, C. Calero, J. Camacho, Advanced Functional Materials p. 3837 (2016)
48. R. Messina, L.A. Khalil, I. Stanković, Physical Review E **89**, 011202 (2014)
49. N. Vandewalle, S. Dorbolo, New Journal of Physics **16**, 013050 (2014)
50. T. Pöschel, T. Schwager, *Computational granular dynamics: models and algorithms* (Springer Science & Business Media, 2005)
51. F. Radjaï, F. Dubois, *Discrete-element modeling of granular materials* (Wiley-Iste, 2011)
52. J.Y. Ooi, V. Magnanimo, J. Sun, S. Luding, Powder technology **293**, 1 (2016)
53. U. Welling, G. Germano, Computer Physics Communications **182**, 611 (2011)
54. N. Pottier, *Physique statistique hors d'équilibre: processus irréversibles linéaires* (EDP Sciences, 2007)
55. Z. Peng, E. Doroodchi, G. Evans, Powder Technology **204**, 91 (2010)
56. A. Li, G. Ahmadi, Aerosol science and technology **16**, 209 (1992)
57. J.N. Israelachvili, *Intermolecular and surface forces: revised third edition* (Academic press, 2011)
58. R. Messina, L. Spiteri, The European Physical Journal E **39**, 81 (2016)